Excited-state dynamics of rare-gas clusters

Dafna Scharf and Joshua Jortner
School of Chemistry, Tel-Aviv University, 69978 Tel-Aviv, Israel

Uzi Landman
School of Physics, Georgia Institute of Technology, Atlanta, Georgia 30332

(Received 14 September 1987; accepted 26 October 1987)

In this paper we explore the dynamic implications of energy exchange in electronically vibrationally excited states of mixed rare-gas clusters. The classical molecular dynamics method was applied for the study of vibrational energy flow from electronically excited atomic $Xe(^3P_1)$ states in Xe^*Ar_{12} and Xe^*Ar_{54}, and the consequences of $Xe_2^*(^3\Sigma_u)$ excimer formation in $Xe_2^*Ar_{11}$ and $Xe_2^*Ar_{53}$ clusters. We have established the occurrence of an ultrafast vibrational energy flow (~ 300 fs) from local Rydberg atomic and excimer excitations into the cluster, which is accompanied by large configurational dilation around the excited state, due to short-range repulsive interactions. Size effects on cluster dynamics were elucidated, being manifested by vibrational predissociation in small clusters and by vibrational relaxation and vibrational energy redistribution in large clusters. A gradual transition from reactive molecular type relaxation in small clusters to nonreactive condensed-matter type relaxation in large clusters was documented. Qualitative and quantitative differences between relaxation of excited species initially located in the interior or on the surface of the cluster were established, being exhibited in the details of the vibrational energy flow. In the case of bulk $Xe_2^*Ar_{53}$, excessive local heating is manifested in cluster melting, which results in mass transport of the excimer to the cluster surface. The many facets of the dynamics of electronically excited mixed rare-gas clusters are amenable to experimental interrogations.

I. INTRODUCTION

The progress in our understanding of the evolution of quantum, thermodynamic, dynamic, and chemical size effects in clusters,[1–4] is expected to provide a central contribution towards the merging between the microscopic and macroscopic points of view in the description of level structure and dynamics from small molecules to condensed phases.[5] The processes of energy acquisition, storage, and disposal in clusters are of particular interest for the elucidation of dynamic size effects in large finite systems, in which continuous variations of the nuclear and the electronic level structure[6] with cluster size occur. In this context, and of considerable importance, is the fate of a vibrational excitation of a molecule embedded in the cluster, or of the cluster intermolecular mode(s), which can be accomplished by collisional excitation, photoselective vibrational excitation, or electronic excitation followed by intramolecular radiationless transition[7] or by exciton trapping.[8,9] In charged clusters, vibrational excitation can originate from ionization followed by hole trapping, as in rare-gas clusters[10–12] as well as in alkali–halide clusters, and from electron attachment to alkali–halide clusters.[13,14] Vibrational energy relaxation in van der Waals molecules and larger clusters falls into two categories:

(i) Reactive vibrational predissociation,[15–26] which results in vibrational–translational, vibrational–rotational, and vibrational–vibrational energy exchange.

(ii) Nonreactive vibrational energy redistribution, resulting in energy exchange between an intramolecular vibration and low frequency intermolecular modes of the cluster.[19]

Extensive experimental and theoretical studies[15–26] of reactive vibrational predissociation of small van der Waals molecules, e.g., HeI_2 or $(N_2O)_2$ focused attention on the reactive channel. A central conclusion emerging from these studies[16] pertains to the failure of the statistical theories of unimolecular reactions to describe vibrational predissociation of small van der Waals molecules. The lack of vibrational energy randomization in small van der Waals molecules provides a touchstone for mode-selective reactive dynamics. Sequential vibrational energy redistribution followed by presumably nonstatistical dissociation seems to be ubiquitous in van der Waals molecules built from polyatomic molecules and in clusters of diatomics,[20–26] e.g., $(C_2H_4)_2$, $(NH_3)_2$, $(benzene)_2$, and $(HF)_n$ $(n = 2–6)$. An apparent ditochomy[26] between the dephasing lifetimes of some van der Waals molecules ($\sim 10^{-12}$ s), which originates from line broadening and their vibrational predissociation lifetimes ($> 10^{-9}$ s)[7] originates from the dominant contribution of the nonreactive vibrational relaxation to dephasing.[26]

Information regarding vibrational energy degradation in larger clusters stems from molecular dynamics (MD) computer simulations[27–29] of the dissociation of ground state Ar_n $(n = 1–6)$ clusters,[19] which can be accounted for in terms of the statistical theory of unimolecular reactions, and which implies vibrational energy randomization in these clusters.[19] Another significant MD study of vibrational energy degradation in clusters involves the dynamic implications of hole trapping, i.e., the formation of R_2^+ dimer ions in

 0021-9606/88/074273-16$02.10

rare gas clusters.[10,11] These MD studies[10,11] demonstrated the occurrence of complete vibrational relaxation of the dimer ion in Xe_{13}^+ clusters on a time scale of 1 ns, with ~ 3 dissociation events of Xe atoms being exhibited on a time scale of 150 ps past ionization. However, these studies, which are of considerable interest for the elucidation of the issue of the effects of fragmentation on the "magic numbers" of rare-gas clusters,[9] did not address the applicability of statistical unimolecular theories. Nevertheless, the observation of a retardation of the fragmentation with increase of cluster size is in accord with such approaches.

The nonreactive and reactive processes induced by the degradation of electronic–vibrational energy into vibrational energy in clusters are of considerable interest. In this context, we have undertaken the study of the dynamical consequences of the trapping of electronic excitations in rare-gas clusters (RGCs). Extensive information is currently available regarding exciton trapping in neat solid and liquid rare gases[7] and of the trapping of electronic–vibrational excitations in impurity pairs in solid and liquid rare-gas alloys.[7] Exciton or excitation trapping in neat heavy rare-gas liquids and solids, or in impurity dimers of heavy rare gases, i.e., Ar, Kr, and Xe, exhibits two-center localization, resulting in the formation of an electronically excited diatomic rare-gas excimer molecule.[7] The localization of atomic impurity excitation in dilute solid and liquid rare-gas alloys was also explored in considerable detail, being accompanied by large local configurational changes.[7] The nature of electronic excitations in pure and mixed RGCs can be inferred from the information currently available regarding the lowest electronic excitations in pure or doped solid and liquid rare gases. The lowest electronic excitations in pure solid and liquid rare gases can be described either in terms of intermediate Wannier states with large central cell corrections, or by strongly perturbed Frenkel excitons.[7] Similarly, the lowest electronic excited states of an impurity atom in liquid and solid rare-gas alloys are amenable to description[7] either in terms of Wannier impurity states with large central cell correction, or a strongly perturbed atomic excitation. Adopting the latter, tight binding description, the lowest electronic excitations R*, of an atom (R = Ar,Kr,Xe) in neat and mixed RGCs can be described in terms of the atomic $^1S_0 \rightarrow {}^3P_1$ and $^1S_0 \rightarrow {}^1P_1$ excitations, which are modified by large nonorthogonality corrections.[7] The energetic separation between these two electronic excitations corresponds to the spin–orbit splitting. This tight binding description of the atomic electronic excitations in RGCs rests on a decidedly molecular picture. An analogous molecular point of view will be adopted for exciton trapping in a neat RGC or excitation trapping in an impurity pair in a mixed RGC, which results in excimer formation. The excimer diatonic molecule R_2^* (R = Ar,Kr,Xe) constitutes a localized state which is characterized by a large binding energy, and which is initially produced in a highly vibrationally excited state. Energy exchange between electronically excited states of impurity atoms or impurity excimers and the cluster atoms in RGCs fall into two classes:

(1) Short-range repulsive interactions between a spatially expanded Rydberg type excitation of R* and R_2^* and the cluster atoms result in vibrational energy flow into the cluster.

(2) Vibrational relaxation of the excimer results in exchange of vibrational energy between the R_2^* internal mode and the cluster intermolecular modes.

In this paper we explore the dynamic implications of energy exchange between an electronically excited rare-gas impurity atom (R*) or excimers (R_2^*) and host RGCs. We have investigated the mechanisms of cluster vibrational excitation induced by vibrational energy flow from R*, due to short-range repulsive interactions, as well as the consequences of excimer formation in RGCs. In our studies, we have applied the classical molecular dynamics method to simulate the dynamical evolution of electronically vibrationally excited states of mixed $XeAr_{n-1}$ and Xe_2Ar_{n-2} clusters (with $n = 13$ and 55). A preliminary report of excimer trapping in neat RGCs was presented previously.[8,28,29] The MD simulations allow for systematic studies with refined temporal and spatial resolution of the following novel dynamic implications of energy exchange in electronically excited RGCs:

(1) Vibrational energy flow from electronically excited R* and electronically vibrationally excited R_2^* into the cluster, which originates from short-range repulsive interactions (for both R* and R_2^*) and from vibrational energy degradation (of R_2^*).

(2) Reactive and nonreactive processes in clusters. The elucidation of the nature of the relaxation process and its dependence on the electronic excitation of R* or R_2^*, on the excess vibrational energy of R_2^*, on the cluster structure, composition, and size is of considerable interest.

(3) Size effects on intramolecular dynamics in clusters. The reactive vibrational predissociation process manifests the dynamic consequences of vibrational energy flow in small clusters, while vibrational relaxation of an excimer in condensed phases can be viewed as nonreactive vibrational energy redistribution. Vibrational energy flow in clusters is expected to undergo a gradual transition from reactive molecular-type behavior in small clusters to nonreactive solid-state type behavior in large clusters, manifesting the transition from molecular to condensed matter relaxation in large finite systems.

(4) Relaxation of surface and bulk states. The vibrational energy flow from an excimer into a cluster is expected to be qualitatively different when the excimer is in the interior of the cluster or when it is located on the cluster surface. Thus, the exploration of clusters provides a new insight into condensed phase dynamics, making contact with surface phenomena. This distinction between bulk and surface dynamics pertains both to reactive processes in small clusters and to nonreactive vibrational relaxation in large clusters.

(5) Configurational cluster relaxation around electronic excitations. The short-range repulsive interaction between the Rydberg type excitation of R* or R_2^* and the neighboring cluster atoms results in cluster dilation around the electronically excited state. Such a local dilation will result in the formation of a "microscopic cavity" or a "bubble" surrounding the electronic excitations in the cluster. The local structural dilation of the cluster around the excited

electronic state is responsible for vibrational energy flow into the cluster. Such configurational relaxation of the cluster bears a close analogy to medium dilation around electronically excited states of impurity atoms in rare-gas solids,[7] which cause large Stokes shifts and are responsible for excessive homogeneous line broadening in absorption.[7] Local dilation effects which are expected in clusters, are also analogous to "bubble" formation around electronically excited states in liquid helium.[7]

(6) Mass transport of electronic excitations in clusters. When nonreactive vibrational energy flow from an electronic excitation of an impurity to the cluster prevails, local heating of the cluster will result in considerable cluster configurational changes. The most extreme configurational change involves cluster melting.[30,31] Under these circumstances significant diffusion of the electronically excited impurity may take place. This mass transport process may be interrogated by the different rates of vibrational relaxation processes in the cluster interior and on the cluster surface.

II. METHOD

Numerical simulations open new avenues for a detailed microscopic exploration of the time evolution and dynamics of large and complex finite systems,[27–32] which are of interest to us. We have employed the classical MD[33–36] method for the study of the dynamics of mixed rare-gas clusters, $XeAr_{12}$, $XeAr_{54}$, Xe_2Ar_{11}, and Xe_2Ar_{53}, following electronic excitation of a Xe atom or the Xe_2 molecule. Figures 1 and 2 portray the electronically excited states of Xe and Xe_2 relevant to the present study. The electronically excited state of the Xe atom was taken to correspond to the allowed (within the *JJ* coupling scheme) $Xe(^3P_1)$ electronic configuration, which will be denoted as Xe*. Cluster induced quenching effects to the metastable $Xe(^3P_2)$ atomic excitation will be disregarded. The Xe_2^* excimer state was taken to be the $^3\Sigma_u$ excimer state (Fig. 2). Again, cluster induced radiationless transitions between different electronic configurations of the excimer[7] will not be considered.

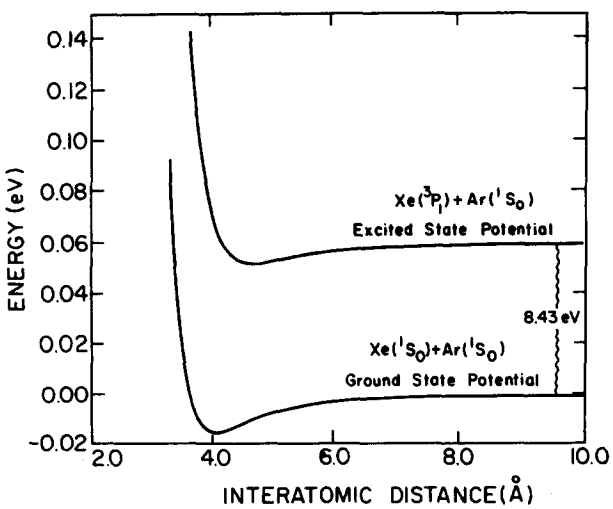

FIG. 1. The potential energy curves for the Xe–Ar potential in the ground and the lowest $^3P_1$ excited electronic states (potential parameters from Ref. 38).

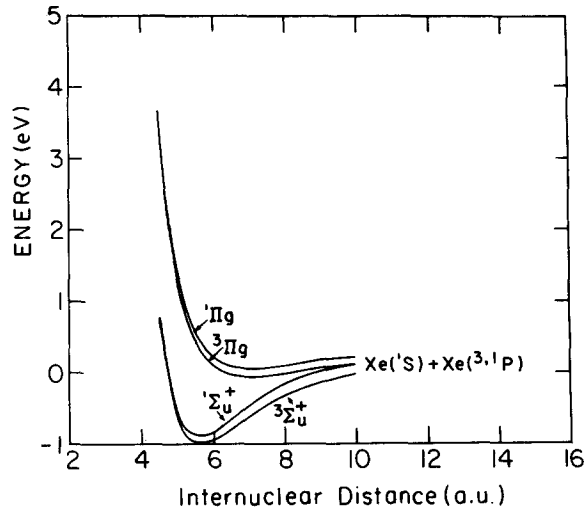

FIG. 2. The four lowest Xe_2^* potential energy curves without spin–orbit coupling. Notice that the lowest $^3\Sigma_u$ and $^1\Sigma_u$ curves lie close to each other and are very similar (from Ref. 40).

In the MD method the phase-space trajectories of a system of interacting particles are generated via the numerical integration of the classical equations of motion. Analysis of these phase-space trajectories allows for the investigations of the structure, energetics and dynamics of the system in equilibrium or under nonequilibrium conditions on refined spatial and temporal scales.

The dynamics of a system of N classical particles of masses $M_I (I = 1,\ldots,N)$, is governed by the system Hamiltonian

$$H = \sum_{I=1}^{N} \frac{\mathbf{P}_I^2}{2M_I} + V(\mathbf{R}_1,\mathbf{R}_2,\ldots,\mathbf{R}_N). \tag{2.1}$$

Assuming pairwise additive central-force interactions, the potential can be written as

$$V(\mathbf{R}_1,\mathbf{R}_2,\ldots,\mathbf{R}_N) = \frac{1}{2}\sum_{I=1}^{N}\sum_{\substack{J=1 \\ I\neq J}}^{N} \phi_{IJ}(R_{IJ}), \tag{2.2}$$

where ϕ_{IJ} are the pair potentials which depend on the distance between the particles I and J, $R_{IJ} = |\mathbf{R}_I - \mathbf{R}_J|$.

For our mixed rare-gas clusters the Ar–Ar and Xe–Ar pair interactions in the ground electronic state were fitted, on the basis of experimental data to the Lennard-Jones (LJ) potential[37–39]:

$$\phi_{IJ}(R_{IJ}) = 4\epsilon_{IJ}\left[\left(\frac{\sigma_{IJ}}{R_{IJ}}\right)^{12} - \left(\frac{\sigma_{IJ}}{R_{IJ}}\right)^{6}\right] \tag{2.3}$$

which is characterized by the energy and distance parameters ϵ_{IJ} and σ_{IJ}, respectively (Table I).

We have used for the elementary units of energy and length the values of the parameters for the Ar–Ar interaction in the ground electronic state, namely $\epsilon/k_B = 120$ K and $\sigma = 3.40$ Å. For the Ar mass, we take $m = 39.95$ amu. The resulting time unit is 1 t.u. $= (m\sigma^2/\epsilon)^{1/2} = 2.142\,63\times10^{-12}$ s.

For the interaction potential between an electronically excited Xe atom (Xe*) in its Xe ($^3P_1$) excited state and a ground state Ar atom, we have used the Lennard-Jones po-

TABLE I. Ground state and excited state Lennard-Jones potential parameters. σ_{IJ} is the interatomic distance at zero potential energy. ϵ_{IJ} is the potential-well depth and R_e is the equilibrium distance.

	σ_{IJ}(Å)	ϵ_{IJ}(K)	R_e(Å)
Ground electronic state:			
Ar–Ar[a]	3.40	120.0	3.71
Ar–Xe[b]	3.65	177.6	3.98
Xe–Xe[c]	4.10	222.3	4.47
Excited electronic state:			
Ar–Xe[b]	4.13	92.8	4.50

[a] Reference 37.
[b] Reference 38.
[c] Reference 39.

tential parameters extracted from spectroscopic measurements of the lowest resonance line of atomic Xe, $Xe(^1S_0) \rightarrow Xe(^3P_1)$ in dense supercritical and subcritical fluid argon[38] (Fig. 1). The excited state $Xe(^3P_1) + Ar(^1S_0)$ pair potential parameters are given in Table I. We have verified that using the LJ potential and alternatively an exponential-6 potential[38] did not lead to noticeable differences in the dynamics of Xe^*Ar_{12}. The same interaction pairwise potential was used for the interaction between each of the two Xe atoms in Xe_2^* and the Ar atoms.

The electronically excited state of the Xe_2^* in the $^3\Sigma_u$ state, Fig. 2, was described by a potential curve of a diatomic molecule which was fitted to a Morse potential:

$$\phi_{IJ} = D_e\left[\exp\left\{-2B\left(\frac{R_{IJ}}{R_e}-1\right)\right\} - 2\exp\left\{-B\left(\frac{R_{IJ}}{R_e}-1\right)\right\}\right], \tag{2.4}$$

where D_e is the dissociation energy, R_{IJ} is the interatomic distance, R_e is the equilibrium distance, and B is a dimensionless parameter. From the spectroscopic data[40] for the $^3\Sigma_u$ state of Xe_2^* we have obtained the following Morse parameters for this state: $D_e = 11\,609$ K ($95.94\ \epsilon_{Ar}/k_B$), $B = 4.228$, and $R_e = 2.999$ Å. The potential parameters for the $^1\Sigma_u$ state (Fig. 2) are similar to those of the $^3\Sigma_u$ state.[40] The interaction between the Ar atoms is not influenced by the electronic excitation of the Xe atom.

Our MD calculations utilized a fifth-order predictor corrector method.[33–36] For each of the systems studied, the first stage in the calculation consisted of an equilibrium stage in the ground electronic state of the cluster. Starting from an initial icosahedral structure, the cluster was heated to a temperature $T \sim 50$ K for a short time [~ 5000 integration time steps (t.s.) where 1 t.s. $= 1.6\times10^{-14}$ s]. This temperature is above the "melting" transition of the cluster.[30,41] Subsequently the cluster was slowly cooled to a temperature of $T = 24$ K, which is below the melting temperature for the cluster under study.[41] This procedure was used in order to "anneal" the cluster configuration, thus allowing each cluster size to achieve its lowest energy, ground state configuration. Subsequently, constant energy trajectories were generated in the equilibrium ground electronic state for a long time (1.5×10^5–2.5×10^5 t.s.) Energy was conserved in our calculations to better than 1 part in 10^6 over a typical run of 1 ns.

In the second stage of the calculation, uncorrelated phase-space configurations were selected out of the ground-state equilibrium phase-space records, and these constituted the set of initial states, which were then subjected to electronic excitation and over which initial state averaging was later performed. The optical excitation was simulated by an instantaneous switching-on of the excited-state potentials in the sampled ground state configuration. This sudden switching-on of the excited-state potentials, corresponds to a vertical Franck–Condon transition to a vibrationally excited state of the electronically excited cluster. We shall refer to this optical excitation as a vertical excitation. The total energy of the cluster was calculated with reference to the energy of a totally dissociated cluster as the zero of the energy scale. Obviously, the total energy in the excited electronic state was higher than the corresponding total energy in the ground state. Following the vertical excitation, the evolution of the system on the excited state potential energy surface starts from a configuration which is far from an equilibrium one for this excited state. Therefore, in order to conserve energy (1 part in 10^6 over a typical run of 1 ns) the integration time step at this stage of the calculation had to be reduced to 1.6×10^{-16} s for the 13 atom clusters and 7.0×10^{-15} s for the 55 atom cluster.

The lifetime of the electronic excitation of $Xe(^3P_1)$—which we are simulating—is of the order of nanosecond, being 3.4 ns for the isolated atom[7] and 2.4 ± 0.2 ns for the Xe in a Ne matrix.[7] The radiative lifetimes τ_2 and τ_1 for the $^3\Sigma_u$ and $^1\Sigma_u$ states, of the Xe_2^* excimer, respectively, are $\tau_2 = 100$ ns and $\tau_1 = 4.6 \pm 0.3$ ns for the free excimer,[7] $\tau_2 \simeq 60$–15 ns and $\tau_1 = 1.3$ ns for solid Xe,[7] while for liquid Xe[7] $\tau_2 = 27 \pm 1$ ns and $\tau_1 = 2.2 \pm 0.3$ ns. The insensitivity of the radiative lifetimes of both the atomic and excimer states to medium effects in the bulk, can be reconciled with a large medium distortion around these Rydberg excitations.[7] On that time scale the cluster will undergo spontaneous decay via fluorescence, to a vibrationally excited ground electronic state. This deexcitation process was modeled by an instantaneous switching-off of the excited state potentials and re-instatement of the ground state potentials in the excited-state configuration.

III. ANALYSIS

The integration of the equations of motion yields the phase-space trajectories as a function of time. The recorded phase-space information yields the time evolution of physical properties for nonequilibrium conditions, as well as equilibrium properties via time averaging over the system trajectories. In this section we describe the analysis of the MD phase-space information, pertaining to the energetics, structure, and dynamics of mixed rare-gas clusters, following electronic excitation.

A. Size analysis

We define the "main fragment" of the parent cluster as the fragment which includes the excited Xe* atom or the

Xe_2^* excimer, together with the Ar atoms close to the electronically excited species. The identification of the constituents of the main fragment is based on a criterion of connectivity with nearest neighbor separation, not exceeding $3\sigma_{IJ}$. This cutoff distance was adopted because the Lennard-Jones interaction beyond this distance is negligibly small. Variations in the number of atoms in the main fragment reflect sequential fragmentations of the cluster. An identical connectivity criterion was used to characterize other fragments consisting of ground state Ar atoms. The dynamical implementation of the connectivity criterion enabled the characterization of time dependence of the size distribution of fragments. Thus we have as time-dependent observables the size of the main fragment and the size and number of any other fragment as well as the total number of fragments in the system. Size analysis was performed in the excited electronic state from $t = 0$, i.e., the excitation event and up to 1 ns, as well as in the ground electronic state following the deexcitation.

B. Energetics

Utilizing the dynamical size analysis information, it is possible to follow the energy flow in the cluster from the excited atom(s) to the rest of the cluster, as well as the energy of each fragment. Denoting by $M(t)$ $(M \leqslant N)$ the instantaneous number of atoms in the main fragment at time t, the energy of the main fragment E_{MF}, is given by

$$E_{\mathrm{MF}}(\{R_{IJ}\},t,M) = \sum_{I=1}^{M} \frac{\mathbf{P}_I^2}{2M_I} + \frac{1}{2} \sum_{\substack{I=J \\ I \neq J}}^{M} \sum_{J=1}^{M} \phi_{IJ}(R_{IJ}). \tag{3.1}$$

The energies of other fragments can be calculated in a similar manner.

The energy of the main fragment was further partitioned into two separate contributions. (i) The energy of the "excitation center" which contains the Xe atom(s) and (ii) the energy of the "bath subsystem," which consists of the Ar atoms in the main fragment. The energy of the excitation center was taken to be the sum of the kinetic energy of the Xe atom(s) and one half of the potential energy between the Xe atom(s) and the Ar atoms. The energy of the Ar bath subsystem atoms was taken as the sum of the kinetic energies of the Ar atoms, the potential energy of Ar–Ar interactions together with one half of the potential energy of interactions of the Ar atoms with the Xe atom(s).

In the clusters $Xe_2^*Ar_{11}$ and $Xe_2^*Ar_{53}$, it is also interesting to follow the energetics of the bare excimer, i.e., the kinetic energy and the potential energy of the excimer atoms. As the system evolves past the electronic excitation, the kinetic energy of the excimer is exchanged with its potential energy, while their sum, i.e., the energy of the bare excimer, decreases with time. This decrease in the energy of the bare excimer interrogates the energy being transferred from the excimer to the cluster.

C. Configurational relaxation

In order to explore structural relaxations we calculated the average distance $\bar{R}(t)$ in the main fragment, between a Xe* atom and the first coordination shell of Ar atoms as a function of time. Denoting by K the number of Ar atoms in the first coordination shell, we take

$$\bar{R}(t) = \left| \frac{1}{K} \sum_{J=1}^{K} [\mathbf{R}_J(t) - \mathbf{R}_{\mathrm{Xe}^*}(t)] \right|. \tag{3.2}$$

In the $Xe_2^*Ar_{11}$ and $Xe_2^*Ar_{53}$ system, these average distances were calculated for each of the Xe atoms, while the neighboring Xe atom was excluded from the summation.

D. Mass transport of electronic excitations

In large clusters $Xe_2^*Ar_{53}$ and Xe^*Ar_{54} the electronically excited species, which is initially located either at the center or on the surface of the cluster, may undergo a mass transport process. We have followed the relative positioning of Xe* or of Xe_2^* relative to the center of mass of the Ar atoms in the main fragment,

$$\mathbf{R}_{\mathrm{CM}}(t) = \sum_{I=1}^{N_{\mathrm{Ar}}} \frac{\mathbf{R}_I(t)}{N_{\mathrm{Ar}}}, \tag{3.3}$$

where N_{Ar} is the number of Ar atoms in the main fragments. The distance between the center of mass of the Ar atoms in the main fragment and the center of mass of the Xe_2^* excimer is

$$\Delta R_{\mathrm{CM}}(t) = |\mathbf{R}_{\mathrm{CM}}(t) - 0.5[\mathbf{R}_{\mathrm{Xe}_1}(t) + \mathbf{R}_{\mathrm{Xe}_2}(t)]|, \tag{3.4}$$

while the corresponding distance from the center of the atomic Xe* excitation is

$$\Delta R_{\mathrm{CM}}^{\mathrm{Xe}}(t) = |\mathbf{R}_{\mathrm{CM}}(t) - \mathbf{R}_{\mathrm{Xe}^*}(t)|. \tag{3.5}$$

IV. RESULTS AND DISCUSSION

A. Atomic impurity excitations in Xe^*Ar_{54} clusters

We have studied the dynamics of Xe^*Ar_{12} and Xe^*Ar_{54} clusters with the Xe atom being initially located either within the "bulk" of the cluster or on the cluster surface. We distinguish between two cases according to the number of Ar atoms in the first coordination shell around the Xe atom. A Xe atom embedded in the cluster and possessing a complete coordination shell of 12 nearest neighbor Ar atoms is referred to as a central bulk Xe atom, while a Xe atom on the periphery of the cluster with a coordination number of 6–7 atoms, which is partially exposed, is referred to as a surface Xe atom.

TABLE II. Total energy (TE) of the clusters in the ground electronic state (g.s.) and in the excited state (e.s.) at $T = 24$ K. Energies are given in ϵ unit of Ar ($1\epsilon = 120$ K $= 0.0105$ eV). Energies were calculated relative to the corresponding totally dissociated cluster which was assigned a zero energy.

	TE (g.s.)	TE (e.s.)
$XeAr_{12}$ (central Xe)	− 41.9	− 19.8
$XeAr_{12}$ (surface Xe)	− 44.4	− 34.2
$XeAr_{54}$ (central Xe)	− 259.8	− 229.8
$XeAr_{54}$ (surface Xe)	− 282.7	− 256.1
Xe_2Ar_{11}	− 44.3	− 33.8
Xe_2Ar_{53} (central Xe_2)	− 267.7	− 243.4
Xe_2Ar_{53} (surface Xe_2)	− 254.5	− 270.3

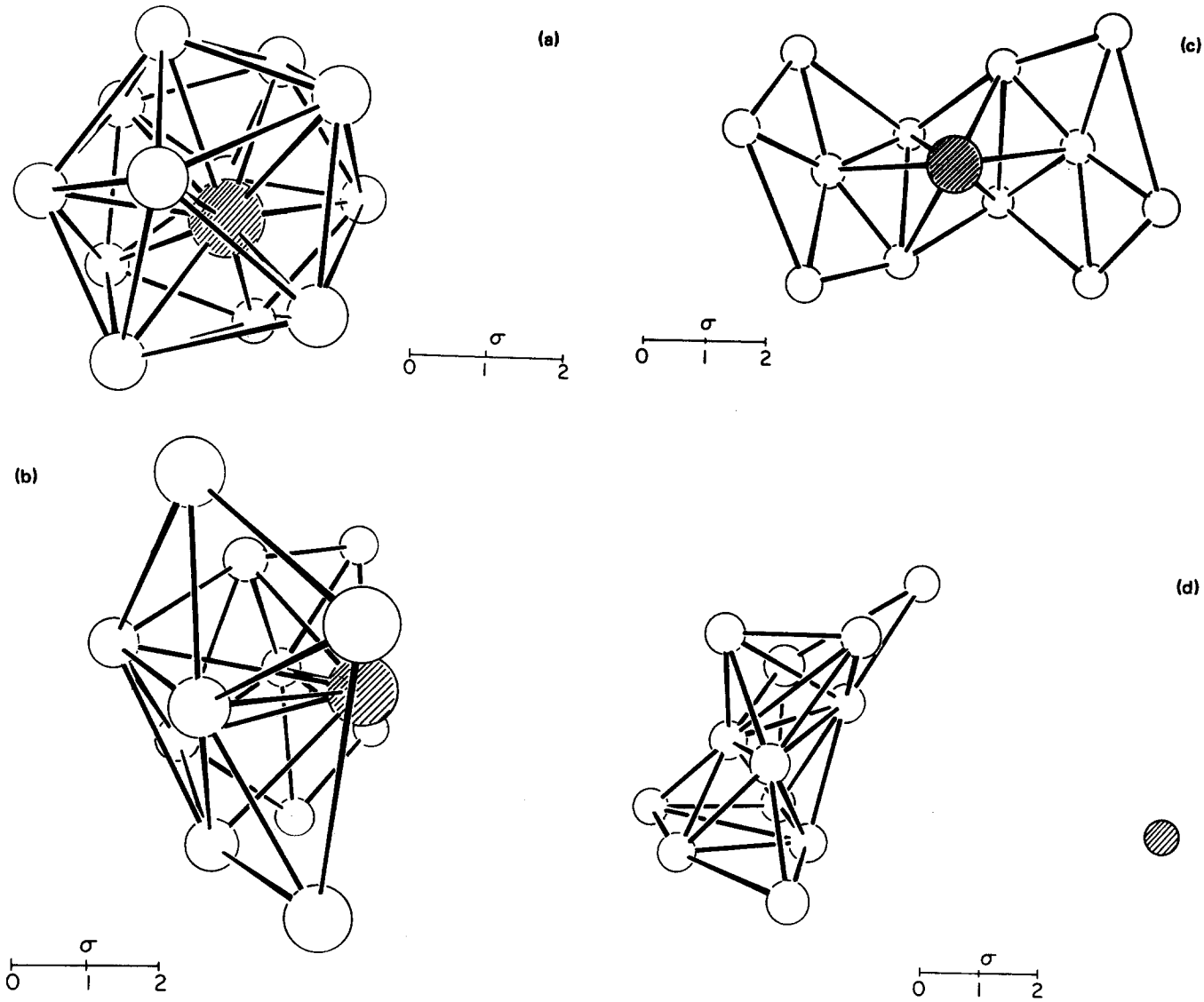

FIG. 3. (a) The ground state $XeAr_{12}$ configuration at $T = 24$ K. Empty and hashed balls correspond to Ar and Xe, respectively. (b) The configuration of the Xe^*Ar_{12} cluster at 1.1 ps past the excitation. (c) The configuration at 5.0 ps past excitation. (d) The configuration after the escape of the Xe* atom at 45 ps past the excitation.

The relative stability of the surface and the bulk $XeAr_{n-1}$ ($n = 13$ and 55) clusters can be assessed from the total energies of these clusters in their ground electronic state and in their vertical electronically excited state (Table II). The surface Xe clusters are energetically more stable than the clusters with the Xe atom in the central position both in the ground state and in the electronically excited state of $XeAr_{n-1}$ ($n = 13,55$). The energetic stability of the ground state of the surface Xe clusters can be rationalized in terms of the lowering of the repulsive Xe–Ar interactions for the surface cluster relative to the bulk cluster. This decrease originates from the lower coordination number in the former case. The contributions of the repulsive interactions are determined by the σ_{IJ} parameters of the LJ potential, which are indeed larger for the Xe–Ar pair interaction than for the Ar–Ar interaction (Table I). Accordingly, the Xe–Ar ground state repulsive interaction will favor the surface configuration in the ground state. The energetic stability of the surface state for the vertical electronically excited state of Xe^*Ar_{12} and Xe^*Ar_{54} can also be rationalized in terms of the enhanced repulsive Xe*–Ar interactions (Table I), which again energetically favor the configuration with the lower coordination number of the Xe atom. These energetic considerations favor the surface configuration both for $XeAr_{n-1}$ and for Xe^*Ar_{n-1} ($n = 13,55$). However, due to kinetic constraints, once a metastable central atom cluster configuration has been produced in a cluster beam, the rate of transformation to the energetically stable surface state is expected to be exceedingly small at low temperatures (24 K), which are of interest to us.

The time evolution of Xe^*Ar_{12} containing a central Xe atom is portrayed in Figs. 3 and 4. Upon the excitation of a central Xe atom in the $XeAr_{12}$ clusters, we observed an ultrafast energy transfer ($\sim 8\epsilon$) from the excitation center containing the Xe* atom to its 12 surrounding Ar atoms, which occurred on a time scale of 350 ± 100 fs (Fig. 4). Subsequently, some of this energy was slowly transferred back (on a time scale up to 20 ps) from the bath subsystem to

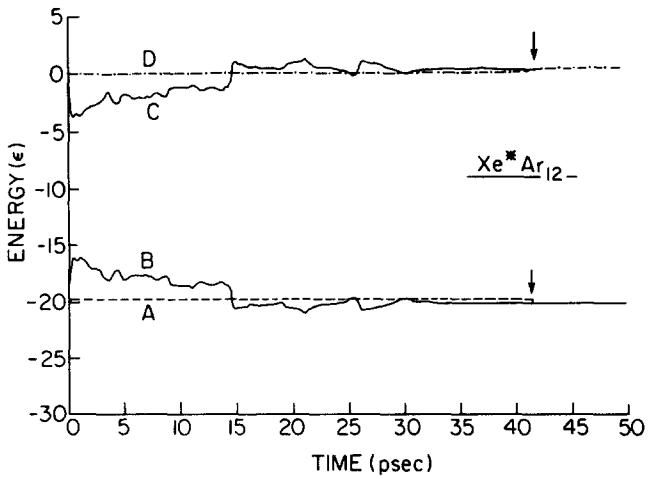

FIG. 4. Energies, in units of ϵ, of a Xe^*Ar_{12} cluster following electronic excitation at $t = 0$. The total energy of the main fragment and that of the Ar bath subsystem are shown in A and B, respectively. In C the total energy of the excitation center is shown and in D the kinetic energy of the dissociated fragment. The arrow marks the time of fragmentation (in this case the escape of the Xe* atom for this sample).

the excitation center containing the Xe atom. Energy exchange resulted in a fragmentation process on a time scale of (55 ± 25) ps, which is manifested in discontinuity (step) in the plots of Fig. 4. Altogether two fragmentations occurred within a time span of 100 ps following the excitation. In the first or second fragmentation event we observed an escape of the central Xe* atom from its surrounding Ar atoms. The kinetic energy of the bare Xe* was $(1 \pm 0.5)\epsilon$. The residual Ar_{11} or Ar_{12} cluster was found to undergo subsequent fragmentations on a time scale of about 300 ps. Major configurational changes precede and accompany the "escape" of the central Xe atom from a Xe^*Ar_{12} cluster (Fig. 3). While in the ground electronic state the Xe atom is located in the center of the icosahedral structure, upon excitation the electronically excited Xe* in Xe^*Ar_{12} caused substantial structural distortions of the cluster, pushing most of the Ar atoms to one side and exposing itself to the surface on a time scale of 5 ps, see Fig. 3. We note that while the configurational relaxation time is long compared to the time scale of the initial energy transfer, it is significantly shorter than the time by which fragmentation events occur.

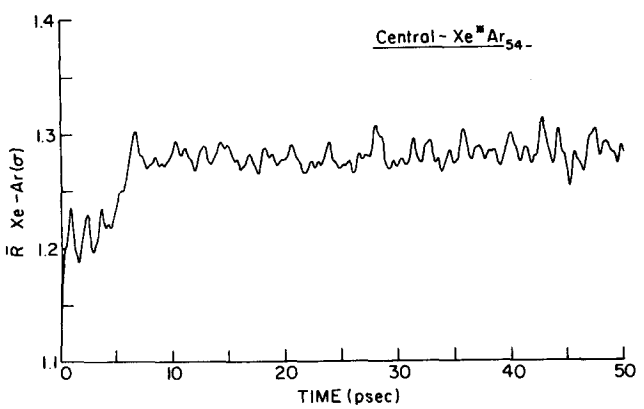

FIG. 5. Time evolution of the average distance, in units of σ, between the central Xe* atom in a Xe^*Ar_{54} cluster and the first Ar atoms coordination shell. The increase from $\sim 1.13\sigma$ to a value of $\sim 1.27\sigma$ corresponds to structural dilation (bubble formation) around the Xe*.

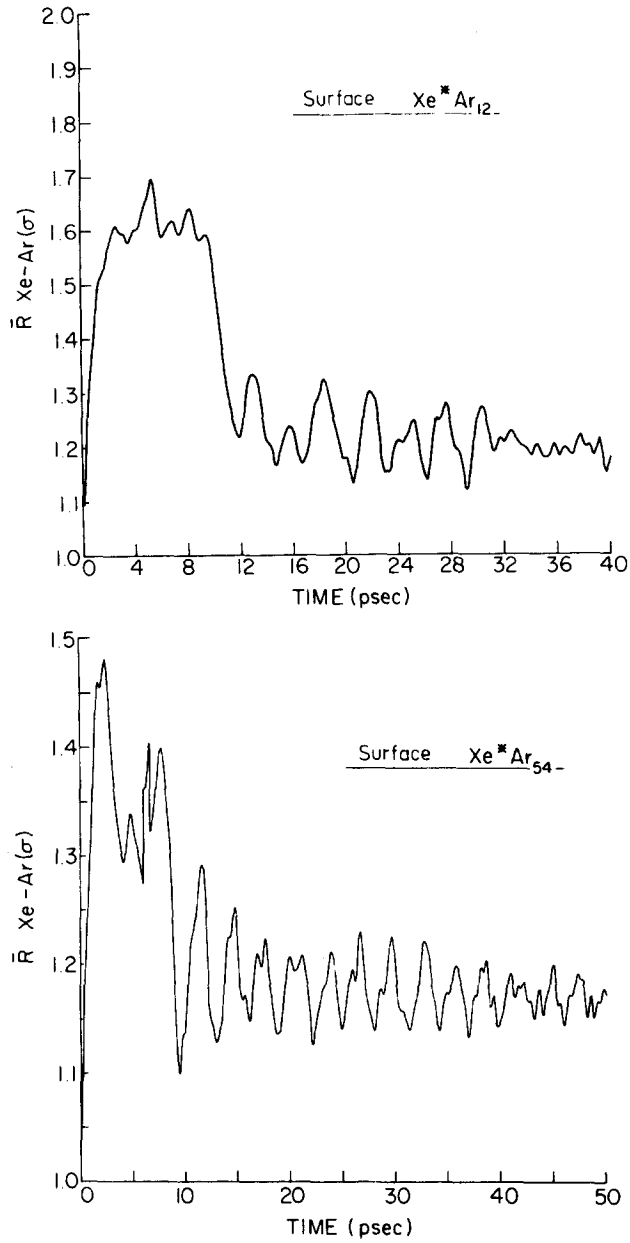

FIG. 6. Time evolution of the average distance, in units of σ, between a surface Xe* atom and its shell of Ar nearest neighbors (a) in Xe^*Ar_{12}, and (b) in Xe^*Ar_{54}.

The dynamics of a large Xe^*Ar_{54} cluster containing a central Xe atom is qualitatively different from that of the corresponding small Xe^*Ar_{12} cluster. The central Xe* atom in Xe^*Ar_{54} clusters remained "trapped" inside the cluster even on a nanosecond time scale past the electronic excitation. Moreover, no fragmentation processes were observed up to these long times in the excited state. Characteristic to these systems is an ultrafast energy transfer at the amount of 9ϵ from the Xe* excitation center to the Ar "bath" subsystem occurring on a 250 ± 100 fs time scale after the excitation. This ultrafast energy transfer process is a consequence of the short-range repulsive interactions between the Rydberg state of Xe* and the neighboring Ar atoms. Subsequent-

ly, on a time scale exceeding 1 ps no major energy flow was observed. Small energy exchanges ($\sim 1\epsilon$) between the "bath" subsystem and the excitation center prevailed on a long time scale of 1–1000 ps. The short-range repulsive interaction between the vertically excited central Xe* and its neighboring Ar atoms result in a major configurational relaxation of the cluster, as is evident from the $\bar{R}(t)$ data of Fig. 5. The initial configurational relaxation resulting in the increase of $R(t)$, Eq. (3.2), to $[\bar{R}(t) - \bar{R}(0)]/\bar{R}(0) = 0.15$ is exhibited on a time scale of 200–300 fs, which is comparable to the time scale of the ultrafast energy exchange in this central cluster. The final cluster configuration with a subsequent increase of $\bar{R}(t)$ to $[\bar{R}(t) - \bar{R}(0)]/\bar{R}(0) = 0.3$ was accomplished on a considerably longer time scale of 5–10 ps (Fig. 5). This configurational relaxation involves a cluster dilation effect, resulting in the formation of a "microscopic cavity" or "bubble" around the atomic Rydberg excitation. This configurational relaxation in the large cluster bears a close analogy to the condensed matter solid and liquid excited state dilation phenomena. The present study of a large finite system provided the temporal details of this structural dilation effect, which is of considerable interest for the elucidation of energy and structure relaxation phenomena of Rydbergs in finite and infinite systems.

No mass transfer of the central Xe* atom in the Xe^*Ar_{54} cluster was observed. We have found that ΔR_{CM}^{Xe}, Eq. (3.5), remained close to zero, with the central Xe atom remaining at the center of the cluster at all times.

A Xe atom on the surface of a small or large cluster is characterized by a partial coordination shell of 6–7 atoms, being partially exposed. We thus expect that energy transfer to the cluster from the repulsive interactions of Ar atoms with the surface Xe* atom will be substantially smaller than those induced by the central Xe*. Consequently we expect that the reactive processes will be retarded in clusters where a surface atom is electronically excited. These expectations are borne out by our results. Similar patterns of behavior were found for a surface atom in the small and large rare-gas clusters, i.e., selective excitation of the surface Xe atom in the cluster does not lead to any fragmentation of the cluster up to a nanosecond past excitation. In surface Xe^*Ar_{12} and in surface Xe^*Ar_{54} the initial energy transfer occurred on a 2 ± 0.5 ps time scale, and during this time only a small amount of energy $(2–3)\epsilon$ was transferred to the "bath" subsystem. We note that the time scale for this energy transfer from the surface Xe is an order of magnitude longer than in the previous case of central Xe in a rare-gas cluster, and the amount of energy transferred is comparatively small. Subsequent processes of energy exchange between the bath subsystem and the excitation center containing the surface Xe* occurred on a time scale of up to 20 ps, after which the bath subsystems attained its quasiequilibrium energy and no further net energy transfer was observed up to a nanosecond.

We conclude that no reactive cluster fragmentation is exhibited for electronically excited surface states in both Xe^*Ar_{12} and Xe^*Ar_{54}. On the other hand, the short-range repulsive interactions of the surface Xe* with its partial coordination shell result in large configurational changes in both small and large clusters. As is apparent from Figs. 6(a) and 6(b) a large initial increase of $\bar{R}(t)$, with $[\bar{R}(t) - \bar{R}(0)]/\bar{R}(0) = 0.4$ is exhibited for both surface Xe^*Ar_{12} and Xe^*Ar_{54}, which occurs on a time scale of 2 ps. This time scale is comparable to the characteristic time for the modest initial energy transfer in these clusters. Subsequently, on a longer time scale of ~ 20 ps, $\bar{R}(t)$ is relaxed to a value of $[\bar{R}(t) - \bar{R}(0)]/\bar{R}(0) = 0.15$. The back movement of the Xe* atom is characteristic for surface states. On the time scale of ~ 20 ps the clusters reached their quasiequilibrium configuration, as well as achieving quasiequilibrium energy distribution. It is interesting to note that the time scale for structural and energetic quasiequilibrium in the surface Xe^*Ar_{n-1} ($n = 13,55$) clusters is practically independent of the cluster size.

Additional results emerging from our calculations are of some interest. The final temperature of the bath subsystem was ~ 30 K, which is below the melting temperature of the clusters. Therefore, we have not encountered a migration of the Xe*, and we conclude that the electronic excitation of a single Xe atom in the $XeAr_{n-1}$ clusters exerts only a small perturbation on the system. We have explored the cluster dynamics following the radiative decay $Xe^*(^3P_1) \rightarrow Xe(^1S_0)$ of the Xe^*Ar_{54} cluster, with the Xe atom being located either in the bulk or on the surface. The radiative decay process was switched on at 1 ns past the initial excitation. No fragmentation following electronic deexcitation was observed.

The molecular dynamics of an electronically excited atomic impurity Rydberg state in rare-gas clusters reveals the following features:

(1) A fast vibrational energy transfer is exhibited, which originates from short-range Xe*–Ar repulsive interaction with a Rydberg excitation. For the central Xe* atom ultrafast energy transfer of $(8–9)\epsilon$ on a time scale of 200–300 fs is exhibited for both small Xe^*Ar_{12} and large Xe^*Ar_{54} clusters. For the surface state this fast energy transfer process is exhibited on a longer (2 ps) time scale, being accomplished by small $(2–3)\epsilon$ energy exchange. This process involves energy transfer from the interatomic Xe*–Ar interaction to Ar–Ar vibrational motion. Such initial energy transfer process due to short range repulsions will be prevalent for Rydberg excitations in clusters.

(2) Large configurational changes occur on a fast time scale following Rydberg excitations in clusters, manifesting the effects of short-range repulsive Xe*–Ar interactions with the Rydberg excitation. In large Xe^*Ar_{54} clusters containing a central Xe* atom a large dilation of the first Ar coordination shell is exhibited on an ultrafast time scale, being accompanied by a subsequent dilation. For a central Xe* state of the small Xe^*Ar_{12} cluster a large configurational cluster distortion is exhibited. Finally, for surface states of large Xe^*Ar_{54} and small Xe^*Ar_{12} a large initial configuration dilation is exhibited on a 2 ps time scale followed by back movement of the Xe* towards the Ar atoms. The initial configurational dilation occurs on a time scale of the initial energy transfer.

(3) Features of reactive dynamics in small clusters vs nonreactive dynamics in large clusters are revealed. In small Xe^*Ar_{12} clusters containing a central Xe* atom the (substantial) vibrational energy flow into the cluster results in

reactive vibrational predissociation, leading to the dissociation of the Xe* atom. In large Xe^*Ar_{54} clusters, the flow of the same amount of vibrational energy does not result in cluster vibrational predissociation on the time scale of the electronic excitation. This phenomena provides us with the first example of the "transition" from reactive dissociative dynamics in small clusters to nonreactive vibrational energy redistribution in large clusters.

(4) There are qualitative differences between the dynamics of bulk and surface excitations in clusters, which are manifested by (i) the different time scales for initial energy exchange, and for initial configurational dilation, which is considerably longer (2 ps) for surface states than for bulk states (0.3 ps); (ii) the different quantities of vibrational energy initially exchanged, i.e., $(8–9)\epsilon$ for bulk states and $(2–3)\epsilon$ for surface states; (iii) the details of subsequent configurational changes; and (iv) reactive predissociation in small Xe^*Ar_{12} clusters is exhibited only for bulk Xe* excitation, while for the surface Xe^*Ar_{12} cluster vibrational predissociation is precluded by the small amount of energy transferred to the cluster.

The distinction between reactive and nonreactive dynamics predicted herein can be subjected to an experimental test. From the experimental point of view the reactive predissociation of the central Xe* atom, which will occur in the small Xe^*Ar_{12} cluster, can be interrogated by optical emis-

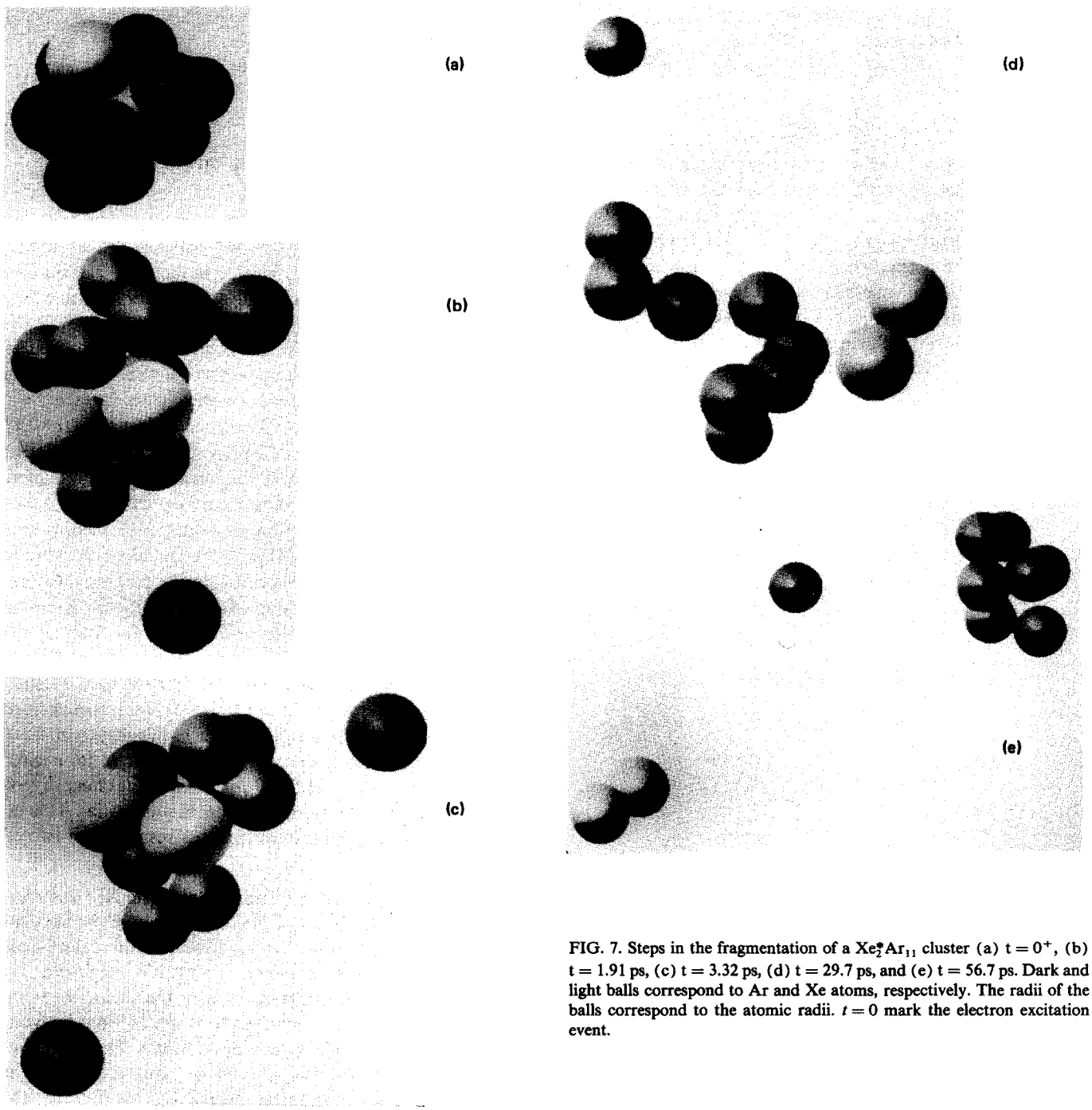

FIG. 7. Steps in the fragmentation of a $Xe_2^*Ar_{11}$ cluster (a) $t = 0^+$, (b) $t = 1.91$ ps, (c) $t = 3.32$ ps, (d) $t = 29.7$ ps, and (e) $t = 56.7$ ps. Dark and light balls correspond to Ar and Xe atoms, respectively. The radii of the balls correspond to the atomic radii. $t = 0$ mark the electron excitation event.

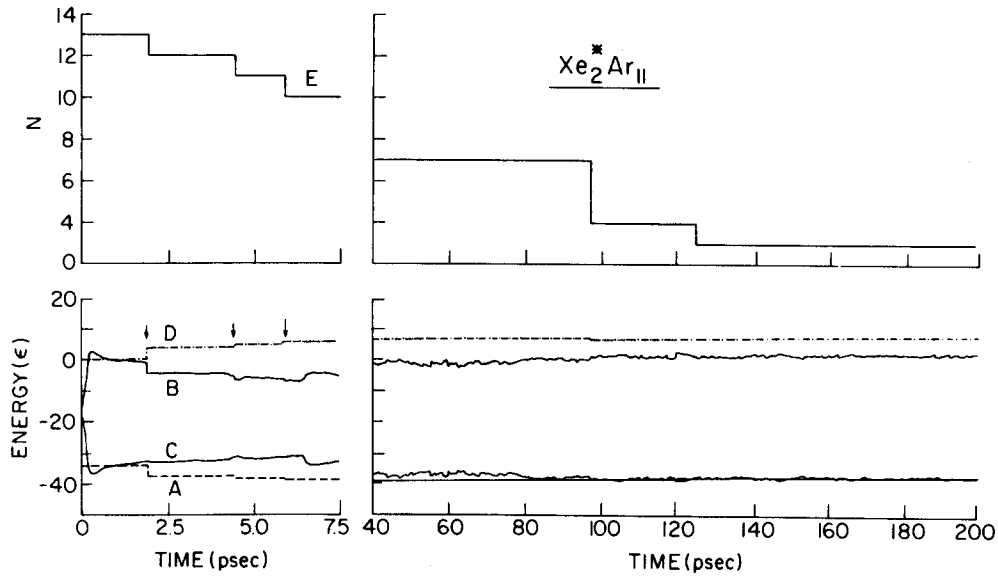

FIG. 8. Time evolution of fragmentation dynamics of the electronically excited $Xe_2^*Ar_{11}$ cluster. (A) Total energy of the main fragment. (B) Total energy of the Ar bath subsystem. (C) Total energy of the Xe_2^* reaction center. (D) Kinetic energy of the dissociated Ar atoms. (E) Number of atoms in the main fragment. The steps in curves (A), (D), and (E) mark the stepwise dissociation of Ar atoms from the main fragment.

sion from the "free" Xe* atom. On the other hand, the emission from either the bulk and surface states from a large Xe^*Ar_{54} cluster as well as from the surface state of Xe^*Ar_{12} will reveal a perturbed emission of Xe*, which is modified by the Xe*–Ar interactions with the dilated or distorted cluster configuration. Another experimental technique for the exploration of the consequences of reactive and nonreactive dynamics of Xe^*Ar_n clusters will involve two-photon ionization mass spectrometry with a vacuum ultraviolet photon exciting the Xe^*Ar_n cluster, whose composition is interrogated by "soft" ionization with a delayed optical laser pulse. This method will provide a clear distinction between the photodissociated Xe* and the main fragment which contains the electronically excited atom.

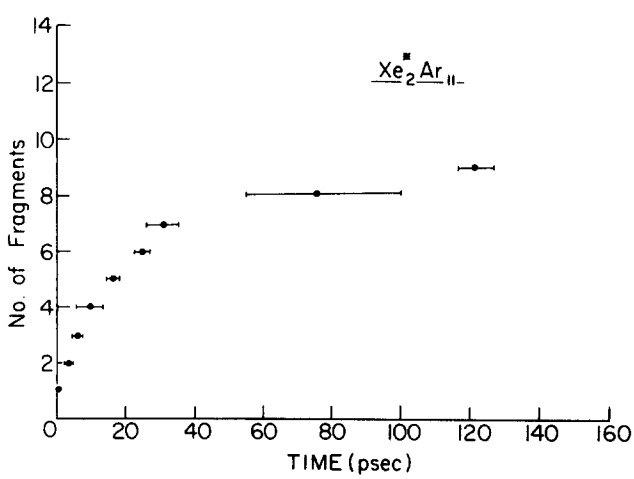

FIG. 9. Number of fragments as a function of time (in ps) for $Xe_2^*Ar_{11}$, averaged over initial equilibrium ground state cluster configurations. The horizontal bars denote the statistical uncertainty of the fragmentation times. Note the change in rate with time.

B. Dynamics of excimer excitations in $Xe_2^*Ar_{11}$ and $Xe_2^*Ar_{53}$ clusters

Vertical excitation of the Xe_2^* excimer in Ar clusters resulted in an electronically vibrationally excited state at the energy of $(20 \pm 2)\epsilon$ below the dissociation limit with excess vibrational energy of $(76 \pm 2)\epsilon$. The ground state Xe–Xe distance and consequently the excimer vertical excitation energy were invariant with respect to whether the Xe dimer is located in the cluster bulk or on the cluster surface.

The vertical electronic–vibrational excitation of the Xe_2^* excimer in the small cluster $Xe_2^*Ar_{11}$ resulted in an efficient vibrational predissociation of the cluster, with a complete dissociation of all the Ar atoms occurring within 200 ps past the excitation process, leaving the bound Xe_2^* excimer in a vibrationally excited state (Figs. 7–9). Detailed information concerning vibrational energy flow in the $Xe_2^*Ar_{11}$ was obtained from the time evolution of the energetic observables, together with the observables pertaining to the dissociation process, which are given in Fig. 8. An ultrafast initial energy transfer process on a time scale of 350 fs to the bath is exhibited, with an energy of $E_t = (18 \pm 2)\epsilon$ being transferred between the excitation center and the bath subsystem. Considering that the total energy of the cluster in its excited electronic state is $(-34.5 \pm 1)\epsilon$, the amount of energy exchanged during the ultrafast process is substantial. This ultrafast efficient energy transfer process results from two effects:

(i) Vibrational energy transfer from the Xe_2^* excimer. The time dependence of the total energy of the bare excimer (Fig. 10) reveals that on the ultrashort time scale of 350 fs the excimer energy is reduced by $E_1 = (9 \pm 1)\epsilon$, being transferred to the bath subsystem.
(ii) Short range repulsive Xe*–Ar interactions between the two excimer atoms and the Ar atoms. The amount of energy transferred due to this process is $E_2 = E_t - E_1 \approx (9 \pm 3)\epsilon$, which is similar to the

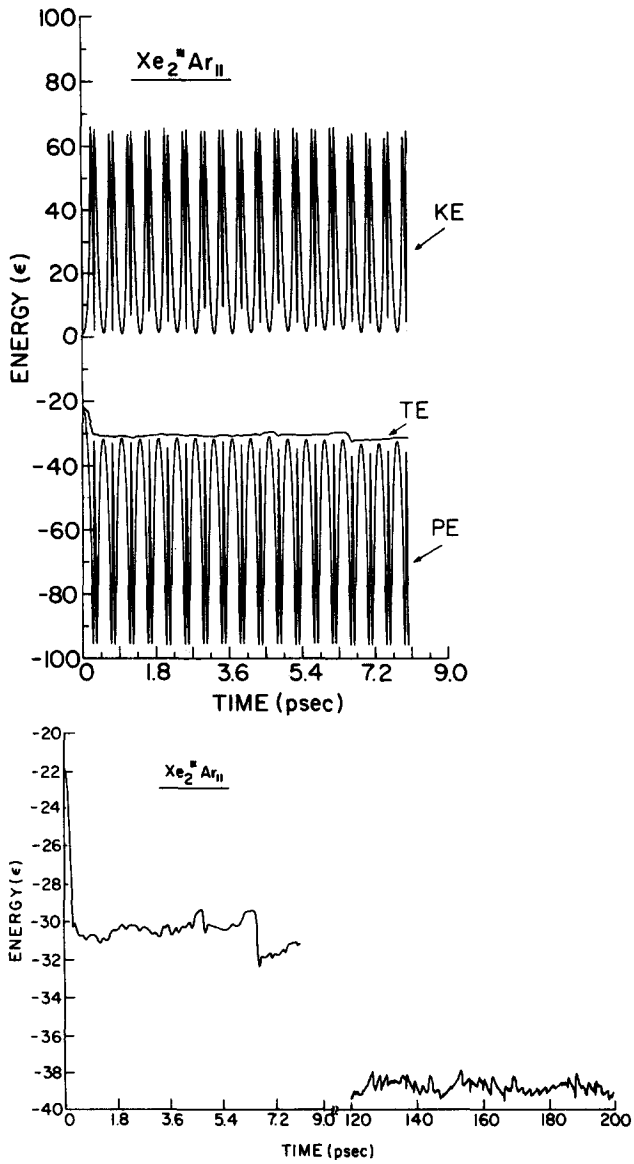

FIG. 10. (a) Time dependence of the potential energy (PE), kinetic energy (KE), and the total energy (TE) of the bare Xe_2^* excimer in $Xe_2^*Ar_{11}$. Energies are in units of ϵ and time in ps. (b) The total energy of the bare Xe_2^* excimer, as shown in (a), and extended to later times.

amount of the ultrafast energy transferred in the bulk Xe^*Ar_{12} cluster.

Processes (i) and (ii) are closely related. Process (i) involves vibrational energy transfer from the intramolecular $(Xe–Xe)^*$ motion to Ar–Ar (and Xe_2^*–Ar) interatomic motion, while process (ii) involves vibrational energy transfer from the interatomic $(Xe–Xe)^*$–Ar potential energy to interatomic Ar–Ar motion. Both processes are induced by short-range Xe_2^*–Ar repulsive interactions and are simultaneously switched-off when configurational relaxation of the small clusters renders these interactions to be small. Subsequent vibrational energy transfer from the excimer to the bath was exhibited on a longer time scale. As is apparent from Figs. 8 and 10 an energy of $(7 \pm 1)\epsilon$ is transferred from the excimer to the cluster on a time scale 1–120 ps.

The ultrafast and subsequent vibrational energy transfer to the small cluster resulted in the dissociation of Ar atoms. The discontinuities in the number of atoms and in the energies of Fig. 8 mark the dissociation of the main fragment, with the decrease of its total energy corresponding to the kinetic energies of the ground state Ar atoms dissociating from it. As apparent from Figs. 8 and 9, the dissociative process involves a stepwise sequential dissociation, i.e., "evaporation" of single ground state Ar atoms from the main fragment. The escape of the excimer from the main fragment was not encountered. The initial ultrafast energy transfer resulted in three consecutive dissociations of Ar atoms on a time scale of 10 ps (Figs. 8 and 9). These initial fragmentations were characterized by high kinetic energies of the dissociating atoms (Fig. 8) of $(3 \pm 1)\epsilon$ per atom. The subsequent fragmentations on the time scale of 10–120 ps were characterized by low kinetic energy of less than 0.5ϵ per fragment. The dynamics of the system ceased at 120 ps, since the excimer was already bare at this state (Fig. 9). Further insight into the energy flow from the excimer into the small cluster is obtained from the time dependence of the kinetic energy, potential energy, and total energy of the excimer (Fig. 10). The strong oscillations in the potential energy and in the kinetic energy clearly indicate the persistence of the vibrational excitation of the excimer over a long time scale.

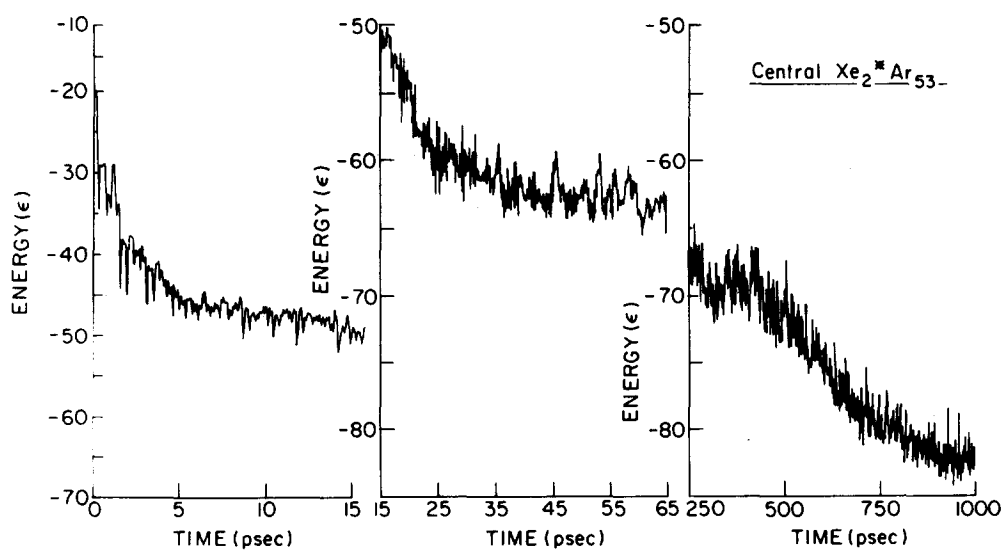

FIG. 11. Total energy of the bare central excimer in $Xe_2^*Ar_{53}$ as a function of time, demonstrating the continuous, prolonged energy transfer to the bath subsystem, following the excitation. The bottom of the Xe_2^* potential well is at $\sim -96\epsilon$. Note the high degree of vibrational relaxation achieved after long times.

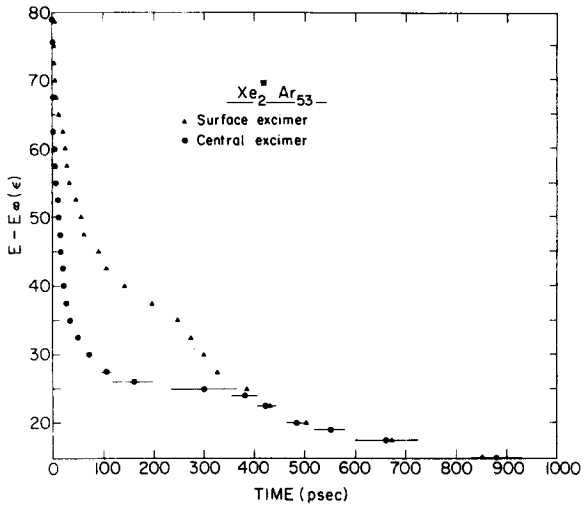

FIG. 12. The excess vibrational energy, in units of ϵ, of the bare Xe_2^* excimer in $Xe_2^*Ar_{53}$ as a function of time. The triangles denote the surface excimer and the dots are for a central excimer. The bars denote span of time for the excimer in a particular average energy. Data are from a single trajectory in each case.

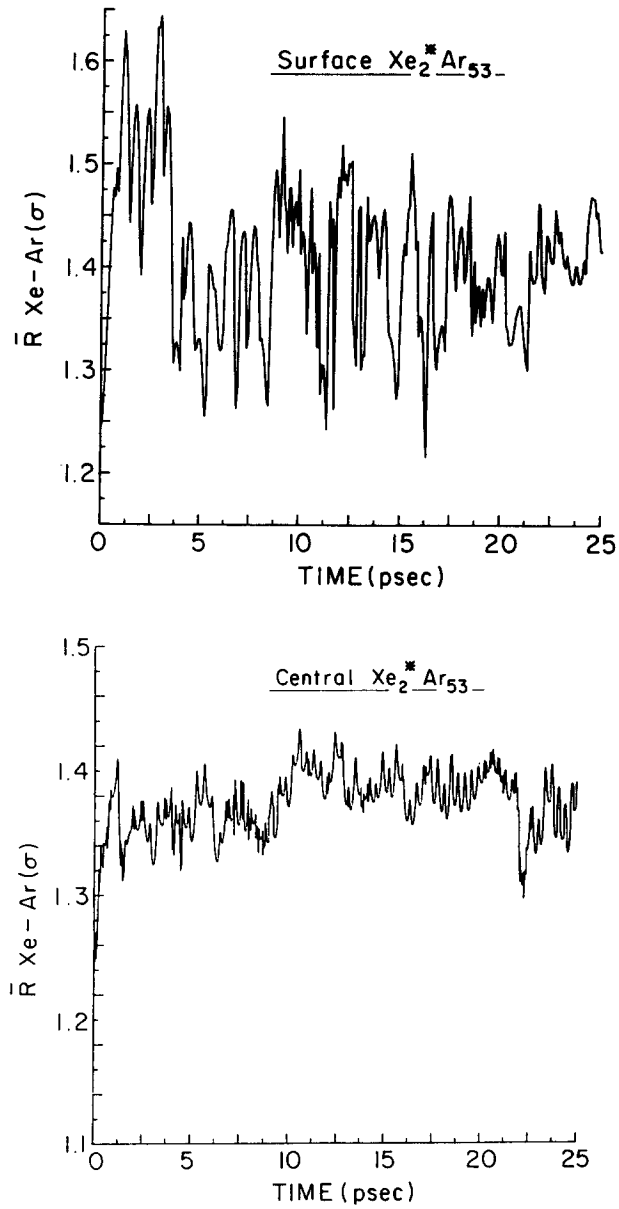

FIG. 13. The average distance, in units of σ, between one of the Xe_2^* excimer atoms and the first Ar coordination shell in $Xe_2^*Ar_{53}$. (a) For a surface excimer and (b) for a central excimer.

As is evident from Figs. 9 and 10, at a time scale exceeding 120 ps when the Xe_2^* excimer is already "liberated," a substantial part of the excitation energy, i.e., $\sim 37\epsilon$ remains trapped as vibrational energy within the isolated Xe_2^* excimer.

For the large $Xe_2^*Ar_{53}$ clusters we have studied the cluster dynamics for the central excimer where the Xe_2 occupies the central cluster site and one site adjacent to it and the surface excimer where the two atoms of Xe_2 are located on the periphery of the cluster. As is apparent from the energetic data of Table II, the central Xe_2Ar_{53} cluster is energetically favored in its ground electronic state, while the $Xe_2^*Ar_{53}$ surface excimer is more stable in the excited electronic state. Electronic–vibrational excitation of the excimer in both the central and surface states results in an initial ultrafast energy transfer process (Figs. 11 and 12) which occurs on a time scale of 350 fs for both central and surface excimers. For the central excimer $E_t = 20\epsilon$ of energy were transferred to the bath subsystem, being accompanied by $E_1 = 12\epsilon$ degradation of the bare excimer energy, while for the surface excimer $E_t = 5\epsilon$ of energy were transferred to the bath subsystem and the bare excimer lost $E_1 \sim 2\epsilon$ of its vibrational energy. This ultrafast energy transfer process, originating both from the partial vibrational relaxation of the excimer and from energy transfer from Xe_2^*–Ar modes to Ar–Ar modes, is induced by short-range Xe_2^*–Ar repulsions. The ultrashort energy transfer is again accompanied by a structural dilation around Xe_2^* for both central and surface excimers occurring on the same time scale (350 fs) (Fig. 13). Both central and surface excimers in the $Xe_2^*Ar_{53}$ clusters exhibited efficient subsequent vibrational relaxation from the excimer to the cluster (Figs. 11 and 12) which proceeds on a time scale of 1–1000 ps. For these large clusters the vibrational relaxation of the excimer is practically complete after 1 ns. The vibrational relaxation process was analyzed in terms of the Bethe–Teller relationship[42,43]

$$\frac{E(t) - E(\infty)}{E(0) - E(\infty)} = \exp(-kt), \tag{4.1}$$

where $E(t)$ and $E(\infty)$ are the energies of the excimer at time t and at the bottom of its potential well, respectively, and k is some characteristic vibrational relaxation rate. Equation (4.1) is applicable for vibrational relaxation of a system of harmonic oscillators. Figures 12 and 14 show the time dependence of $[E(t) - E(\infty)]$ for the central and surface excimers. The initial rate of vibrational energy transfer is faster for the central excimer than for the surface excimer, as expected from the higher coordination number and shorter (initial) bond lengths for the bulk impurity state. The surface excimer reveals a reasonably monotonous, though not strictly linear, Bethe–Teller behavior (Fig. 14) indicating that structural changes are not exhibited during this excimer vibrational relaxation process. The relaxation pattern of the central $Xe_2^*Ar_{53}$ is more complex (Fig. 14), exhibiting a re-

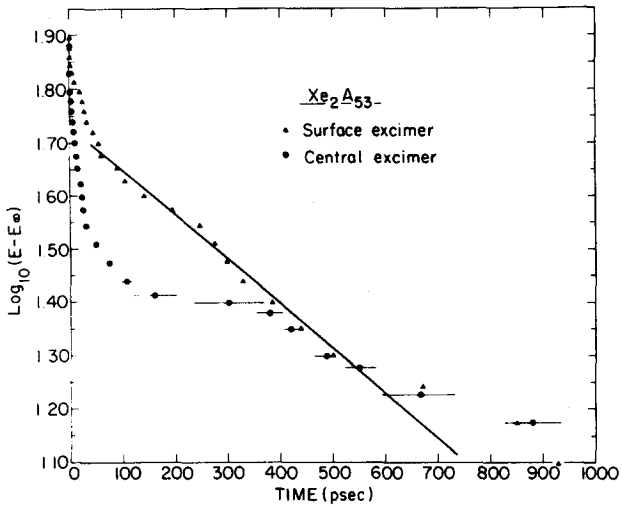

FIG. 14. A Bethe–Teller logarithmic plot of the excess vibrational energy of the bare Xe_2^* excimer in $Xe_2^*Ar_{53}$ as a function of time. The notations are as in Fig. 12.

tardation of the excimer vibrational relaxation process on the time scale 60–300 ps, while for later times a more efficient vibrational relaxation is resumed at a rate which is very similar to that of the surface excimer. This vibrational relaxation behavior of the large cluster, with the central excimers being initially excited, points towards configurational changes in this cluster. A major structural change in the central $Xe_2^*Ar_{53}$ was discovered, which involves the migration of the Xe_2^* excimer to the cluster surface and its eventual partial exposure (Figs. 15 and 16). This excimer migration

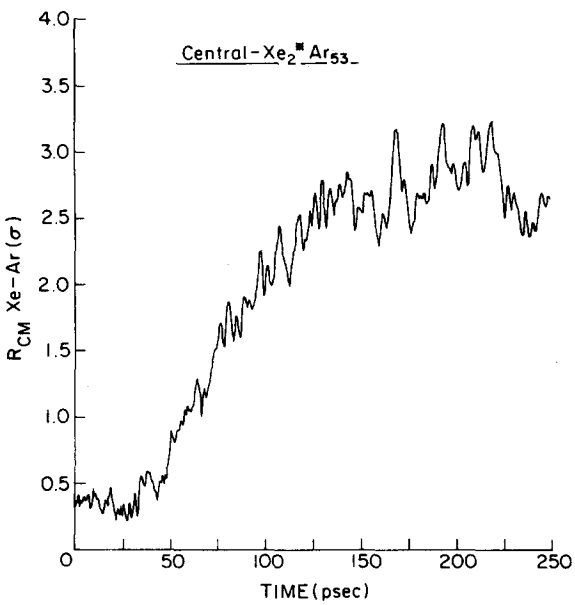

FIG. 15. Excimer migration: The time evolution of the distance between the corresponding centers of mass of the excimer and of the bath subsystem in central $Xe_2^*Ar_{53}$. Initially, the central excimer was near the center of mass of the bath subsystem. The migration of the excimer to the surface of the cluster begins on a time scale of 60 ps past the excitation, and completes in ~200 ps.

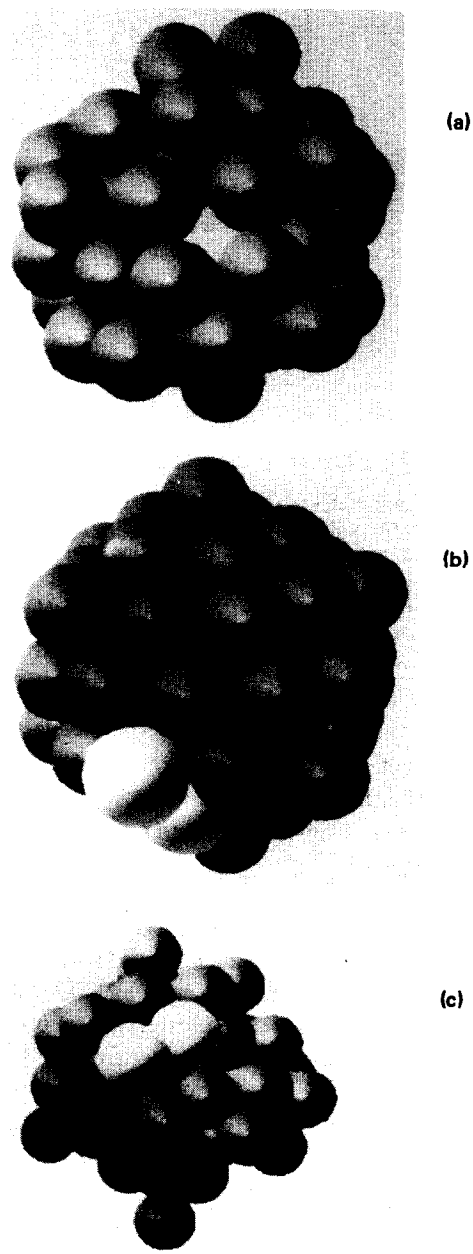

FIG. 16. Snapshots of $Xe_2^*Ar_{53}$ (a) central excimer at time $t=0$ (excitation time), (b) surface excimer at time $t=0$, (c) final state for both (a) and (b) after 1 ns.

process was documented by the dramatic increase of $\Delta R_{CM}(t)$, Eq. (3.4), on the time scale of 50–150 ps (Fig. 15) past the excitation process. The mass transfer of the excimer is facilitated by the "melting" of the large cluster. The energy E_t transferred to in the central $Xe_2^*Ar_{53}$ cluster at $t\sim 50$ ps when the excimer migration sets in (Figs. 11 and 17) was found to be $E_t \sim 45\epsilon$, and the temperature of the cluster can be estimated at $T=0.49\ \epsilon/k_B$. This cluster temperature is above the melting temperature of Ar_{55}.[30] Accordingly, at $t>50$ ps the temperature of the central $Xe_2^*Ar_{53}$ is sufficiently high so that diffusive mass transfer can occur. The unidirectional migration of the central Xe_2^* to the surface can be rationalized on the basis of the energetic data for these clusters (Table II). In the ground electronic state, the central

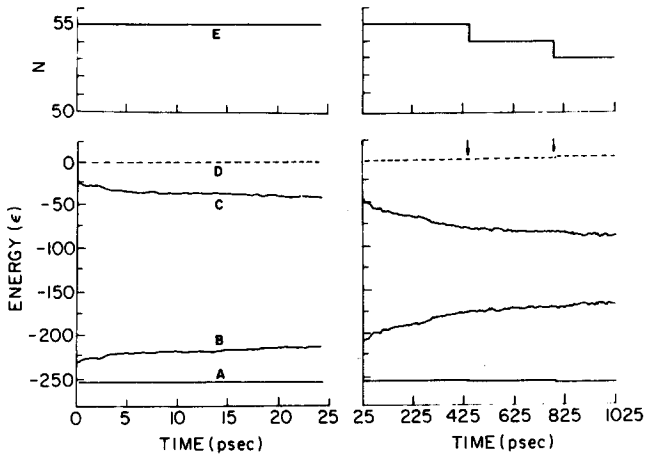

FIG. 17. Time evolution of fragmentation dynamics of the electronically excited central excimer in $Xe_2^*Ar_{53}$ cluster. (A) Total energy of the main fragment, (B) total energy of the bath subsystem, (C) total energy of the reaction center, (D) the kinetic energy of the dissociated Ar atoms, and (E) the number of atoms in the main fragment. The steps in curves (A), (D), and (E) mark the stepwise dissociation of Ar atoms from the main fragment.

Xe_2Ar_{53} cluster is energetically favored in the cluster formation process. On the other hand, the surface $Xe_2^*Ar_{53}$ cluster is more stable, so that mass transfer of Xe_2^* to the surface is energetically favored.

Finally, we focus on the fragmentation dynamics of the large $Xe_2^*Ar_{53}$ cluster. Minor fragmentation occurring on a long time scale was exhibited (Fig. 17). The initial two fragmentation events were exhibited on the time scale 300–700 ps, when the energy transferred to the cluster was $\sim 60\epsilon$, while additional one or two fragmentations occurred on the time scale of 700–1000 ps. The drastic retardation of the reactive vibrational predissociation in large clusters is just the result expected on the basis of the statistical unimolecular rate theory.

The radiative decay process of $Xe_2^*Ar_{53}$ was simulated by switching on the ground electronic state potentials at the time 1 ns past the excitation. Since both the bulk and surface excimer in $Xe_2^*Ar_{53}$ terminates at the surface state at this time of 1 ns, the radiative decay was performed for the surface excimer. Within 1 ± 0.5 ps past the radiative decay the ground state Xe_2 dimer dissociates with one of the Xe atoms leaving the main fragment, while the second Xe atom dissociated within 3 ± 1 ps after the deexcitation. The kinetic energy of the dissociated Xe atoms was $(3 \pm 1)\epsilon$ per atom, being somewhat larger for the first dissociated Xe atom. Since prior to the deexcitation the excimer had only a small excess of vibrational energy we expect that our result of atomic Xe dissociations will be borne out by the physical clusters where the lifetimes of the $Xe_2^*(^3\Sigma_u)$ excimer are expected to be in the range of ~ 20 ns.

Our studies of the molecular dynamics of electronically vibrationally Xe_2^* excimers in Ar clusters reveal:

(1) Ultrafast vibrational energy flow from the Xe_2^* excitation center to the Ar bath subsystem which is induced by short-range repulsive interactions was documented. This process involves two distinct phenomena (i) intermolecular exchange of energy from Xe_2^*–Ar repulsive energy to Ar–Ar motion and (ii) vibrational relaxation of the intramolecular vibrational excitation of Xe_2^*. The vibrational energy transferred by processes (i) and (ii) into the cluster is practically independent of the cluster size. Process (i) is analogous to that encountered for the vibrational energy flow in the atomic excited Xe^*Ar_{n-1} ($n = 13$ and 55) clusters. This initial efficient vibrational energy flow is terminated by structural relaxation.

(2) Configurational dilation of the cluster around the Rydberg type excimer excitation is exhibited both for small and large clusters on the time scale of the ultrafast vibrational energy flow, again in analogy with atomic excitation in Xe^*Ar_{54} and Xe^*Ar_{12} clusters.

(3) Subsequent vibrational energy relaxation of the excimer in these clusters. The size dependence of this vibrational relaxation process is quite marked, i.e., on the time scale of 1–100 ps the main fragment resulting from electronic excitation in small $Xe_2^*Ar_{11}$ cluster dissipates $\sim 8\epsilon$ of the excimer energy while the vibrational relaxation of the main fragment in large $Xe_2^*Ar_{53}$ cluster amounts to the dissipation of $\sim 35\epsilon$ of energy. The enhanced vibrational relaxation efficiency in the large cluster relative to the small cluster on the relevant time scale prior to the fragmentation of the small cluster may originate from its stability with respect to vibrational predissociation. At long times $t \leqslant 1000$ ps vibrational relaxation of the excimer in Xe_2^* proceeds monotonically, with complete vibrational energy relaxation being achieved at 1 ns.

(4) Mass transfer of the central Xe_2^* excimer in large $Xe_2^*Ar_{53}$ was documented. This process is facilitated by cluster "melting."

(5) The distinction between bulk and surface excimer relaxation of the large $Xe_2^*Ar_{53}$ cluster is exhibited at the initial stages ($t \leqslant 50$ ps) of the dynamics, when the initial vibrational energy flow and the subsequent vibrational relaxation of Xe_2^* are more efficient for the bulk state. At longer times mass transport of the central Xe_2^* to the surface of the $Xe_2^*Ar_{53}$ cluster masks the difference between the initial configurations of these large excimer clusters.

(6) The quantitative and qualitative distinctions between the dynamics of excimer and atomic Rydberg excitations pertain to the features related to the vibrational relaxation of the excimer. These involve the higher efficiency of the ultrafast vibrational energy flow in Xe_2^* clusters, the inefficiency of subsequent vibrational energy flow from the excitation center into the bath subsystem past the initial energy exchange process. Another difference between the atomic and excimer excitation in large clusters pertains to the lack of mass transfer of the atomic excitation. The energy flow into the Xe^*Ar_{54} cluster is insufficient to induce a transition into a nonrigid cluster structure, which will facilitate diffusion of the atomic excitation.

(7) Marked deviations from "statistical" vibrational energy redistribution are exhibited in the small $Xe_2^*Ar_{11}$ cluster. The mismatch between the higher vibrational frequency of the excimer and the lower intermolecular vibrational modes of the main fragment results in the persistence of substantial vibrational excitation of the excimer up to the

completion of the cluster fragmentation process. This constitutes an example for the dynamic consequences of "mode selective" vibrational excitation in a cluster.

(8) Reactive dynamics of these clusters involves stepwise consecutive dissociation of single Ar atoms.

(9) Size effects on cluster dynamics. The dynamic consequences of vibrational energy flow into the $Xe_2^*Ar_{n-2}$ ($n = 13,55$) cluster are drastically different for small and large clusters. Reactive vibrational predissociation is prevalent for small $Xe_2^*Ar_{11}$ clusters, resulting in a complete dissociation of the Ar atoms on a time scale of ~ 120 ps. In contrast, the large $Xe_2^*Ar_{53}$ cluster exhibits only a small number (~ 3 events) of Ar fragmentations on the long time scale of 300–1000 ps. The major dynamic process in the large cluster involves nonreactive vibrational relaxation. The qualitative change from dissociation dynamics in $Xe_2^*Ar_{11}$ to vibrational energy redistribution in $Xe_2^*Ar_{53}$ reflects the gradual transition from molecular type reactive dynamics in small clusters to nonreactive condensed matter type dynamics in large clusters. To provide a heuristic description of the size effects on dynamics we assume effective vibrational energy redistribution within the cluster modes (excluding the excimer), prior to any dissociation which is supported by the smooth time dependence of the cluster temperature. We then invoke the simple version of the statistical unimolecular theory for the time τ_D for the first cluster dissociation event

$$\frac{1}{\tau_D} = A\left(\frac{E_v - E_t}{E_v}\right)^{s-1}, \tag{4.2}$$

where A is a frequency factor, E_t is the threshold energy, E_v is the excess vibrational energy, and s is the number of vibrational degrees of freedom. For large s, which is of interest to us, Eq. (4.2) results in a simple rate equation

$$1/\tau_D = A\exp(-E_t/kT_{\text{eff}}) \tag{4.3}$$

with the effective temperature

$$kT_{\text{eff}} = E_v/s - 1. \tag{4.4}$$

The first dissociation time depends, of course, on the cluster size and its excess vibrational energy. The MD data reveal that the first dissociation in $Xe_2^*Ar_{11}$ occurs at $\tau_D = 2.5 \pm 0.5$ ps when the cluster excess vibrational energy is $E_v \sim 20\epsilon$, while for $Xe_2^*Ar_{53}$ we obtained $\tau_D = 400 \pm 100$ ps when $E_v \simeq 60\epsilon$. The ratio of the τ_D values can be accounted for in terms of Eq. (4.3) with the parameters $E_t = 5\epsilon$, which reproduces faithfully the binding energy of a surface Ar atom, while the absolute values of τ_D result in the reasonable value of $A = 2\times 10^{15}\ \text{s}^{-1}$. Accordingly, the reactive dissociative process will be practically switched-off when $\tau_D \gtrsim \tau_{\text{rad}}$, where $\tau_{\text{rad}} = 10$ ns is a characteristic radiative excimer decay lifetime in the electronically excited $^3\Sigma_u$ or $^1\Sigma_u$ state. This state of affairs will prevail for $E_v = 50\epsilon$ when $s \gtrsim 170$, i.e., $n \gtrsim 60$, which provides the signature for the transition for molecular to condensed matter vibrational dynamics in clusters.

Note added in proof: Recent experimental studies of size effects on excited-state dynamics of rare-gas clusters [E. T. Verkhovtseva, E. A. Bondarenko, and Yu. S. Doronin, Chem. Phys. Lett. **140**, 181 (1987)], as interrogated by VUV emission spectroscopy, provide evidence for the occurrence of the gradual transition from reactive relaxation in small clusters to nonreactive relaxation in large clusters. These experimental data for neat Ar_n and Kr_n clusters reveal the dominance of resonance atomic ($^{1,3}P_1 \rightarrow {}^1S_0$) emission and emission from weakly bound excited dimers ($B\,{}^1\Sigma_n^+ \rightarrow X\,{}^1\Sigma_g^+$) for $n \simeq 20$, pointing towards the occurrence of dissociative dynamics in small clusters. Relaxed ($A\,{}^{1,3}\Sigma_u^+ \rightarrow X\,{}^1\Sigma_g^+$) emission from strongly bound excimers is exhibited at $n \gtrsim 50$, demonstrating the occurrence of vibrational relaxation in large clusters. For mixed clusters of Kr in Ar, both atomic Kr ($^{1,3}P_1 \rightarrow {}^1S_0$) and Kr_2 ($A\,{}^{1,3}\Sigma_u \rightarrow X\,{}^1\Sigma_g^+$) emission is exhibited at $n \simeq 50$ which also demonstrates the occurrence of configurational and vibrational relaxation in the large mixed clusters.

ACKNOWLEDGMENTS

This research was supported by the U.S.–Israel Binational Science Foundation and by the U.S. Department of Energy, Grant No. FG05-86ER45234.

[1]Proceedings of International Meeting on Small Particles and Inorganic Clusters, J. Phys. (Paris) Colloque C-2 **38** (1977).
[2]Proceedings of the Second International Meeting on Small Particles and Inorganic Clusters Lausanne, 1980, Surf. Sci. **106**, 1–608 (1981).
[3]Proceedings of Bunsengesellschaft Discussion Meeting on Experiments on Clusters, Koningstein, 1983, Ber. Bunsenges. Phys. Chem. **88** (1984).
[4]Proceedings of the Third International Meeting on Small Particles and Inorganic Clusters, Berlin 1985 Surf. Sci. **156**, 1–1072 (1985).
[5]J. Jortner and R. D. Levine, *Photoselective Chemistry*, edited by J. Jortner, R. D. Levine, and S. A. Rice (Wiley, New York, 1981), p. 1.
[6]J. Jortner, Ber. Bunsenges. Phys. Chem. **88**, 188 (1984).
[7]N. Schwentner, E. E. Koch, and J. Jortner, *Electronic Excitations in Condensed Rare Gases* (Springer, Berlin, 1985).
[8]D. Scharf, J. Jortner, and U. Landman, Chem. Phys. Lett. **126**, 495 (1986).
[9]H. Haberland, Surf. Sci. **156**, 305 (1985).
[10]J. J. Sâenz, J. M. Soler, and N. Garcia, Surf. Sci. **156**, 121 (1985).
[11]J. J. Sâenz, J. M. Soler, N. Garcia, and O. Echt, Chem. Phys. Lett. **109**, 71 (1984).
[12]E. E. Polymeropoulos and J. Brickmann, Surf. Sci. **156**, 563 (1985).
[13]U. Landman, D. Scharf, and J. Jortner, Phys. Rev. Lett. **54**, 1860 (1985).
[14]D. Scharf, U. Landman, and J. Jortner, J. Chem. Phys. **87**, 2716 (1987).
[15]D. H. Levy, Adv. Chem. Phys. **47**, 323 (1981).
[16]A. Beswick and J. Jortner, Adv. Chem. Phys. **47**, 363 (1981).
[17]K. C. Janda, Adv. Chem. Phys. **60**, 201 (1985).
[18]A. Amirav, U. Even, and J. Jortner, J. Chem. Phys. **75**, 2489 (1981).
[19]J. W. Brody and J. D. Doll, J. Chem. Phys. **73**, 2767 (1980).
[20]M. F. Vernon, J. M. Lisy, A. S. Kwok, D. J. Krajnovich, A. Tramer, Y. R. Shen, and Y. T. Lee, J. Phys. Chem. **85**, 3327 (1981).
[21]T. E. Gough, R. E. Miller, and G. Scoles, J. Chem. Phys. **69**, 1588 (1978).
[22]M. P. Casassa, D. S. Bomse, J. L. Beauchamp, and K. C. Janda, J. Chem. Phys. **72**, 6805 (1980).
[23]M. A. Hoffbauer, K. Liu, C. F. Giese, and W. R. Gentry, J. Chem. Phys. **78**, 5567 (1983).
[24]M. J. Howard, S. Burdenski, C. F. Giese, and W. R. Gentry, J. Chem. Phys. **80**, 4137 (1984).
[25]A. Mitchell, J. J. McAuliffe, C. F. Giese, and W. R. Gentry, J. Chem. Phys. **83**, 4271 (1985).
[26]R. D. Johnson, S. Burdenski, M. A. Hoffbauer, C. F. Giese, and W. R. Gentry, J. Chem. Phys. **84**, 2624 (1986).
[27]R. W. Hockney and Y. W. Eastwood, *Computer Simulation Using Particles* (McGraw-Hill, New York, 1981).
[28]U. Landman, R. N. Barnett, J. Luo, D. Scharf, and J. Jortner, in *Few and Many Body Systems and Multiparticle Dynamics*, edited by D. A. Micha (AIP, New York, 1987).

[29]U. Landman, R. N. Barnett, C. L. Cleveland, D. Scharf, and J. Jortner, J. Phys. Chem. **91**, 4890 (1987).
[30]G. Natanson, F. Amar, and R. S. Berry, J. Chem. Phys. **78**, 399 (1983).
[31]J. Jellinek, T. L. Beck, and R. S. Berry, J. Chem. Phys. **84**, 2783 (1986).
[32]F. Abraham, J. Vac. Sci. Technol. B **2**, 543 (1984).
[33]C. W. Gear, The Numerical Integration of Ordinary Differential Equations of Various Orders, Argonne National Laboratory Report, ANL 7126 (1966).
[34]A. Rahman, Phys. Rev. A **136**, 405 (1964).
[35]A. Nordsieck, Math. Comput. **16**, 22 (1962).
[36]A. Rahman and F. H. Stillinger, J. Chem. Phys. **55**, 3336 (1971).
[37]W. D. Kristensen, E. J. Jensen, and M. J. Cotterill, J. Chem. Phys. **60**, 4161 (1974).
[38]I. Messing, B. Raz, and J. Jortner, J. Chem. Phys. **66**, 2239, 4577 (1977).
[39]A. E. Shwerwood and J. M. Prasunitz, J. Chem. Phys. **41**, 429 (1964).
[40]W. C. Ermler, Y. S. Lee, K. S. Pitzer, and N. W. Winter, J. Chem. Phys. **69**, 976 (1978).
[41]N. H. Tsai and E. F. Abraham, Surf. Sci. **77**, 465 (1978).
[42]H. A. Bethe and E. Teller, Deviation from Thermal Equilibrium, Ballistic Research Laboratory Rept. X-117 (1941).
[43]E. W. Montroll and K. E. Shuler, J. Chem. Phys. **26**, 454 (1957).